Available online at www.sciencedirect.com
SCIENCE DIRECT®
Computational Materials Science 37 (2006) 42–50
COMPUTATIONAL MATERIALS SCIENCE
www.elsevier.com/locate/commatsci

Crack-tip stress–strain fields in single crystal nickel-base superalloys at high temperature under cyclic loading

N. Marchal, S. Flouriot, S. Forest *, L. Remy

Centre des Matériaux, Ecole Nationale Supérieure des Mines de Paris, ARMINES—CNRS UMR 7633, BP 87, 91003 Evry Cedex, France

Abstract

This work is related to life prediction of high-pressure single crystal turbine blades. Stress and strain fields are first analysed at the tip of a static crack subjected to creep-fatigue loading, assuming an elasto-viscoplastic single crystal behaviour model. Local ratchetting effects are observed, depending on the distance from the crack-tip. Creep-fatigue loadings are compared with pure fatigue and pure creep loadings. The significant differences are pointed out, especially stress relaxation and amount of plastic slip. These results will be useful for the development of a new life prediction tool, based on local approach to fracture.

Keywords: Crack; Single crystal; Superalloy; Creep-fatigue; Stress–strain field; High temperature

1. Introduction

Improving the life prediction of high-pressure turbine blades in land-gas turbines and aerojet-engines is possible. Such blades are subjected to damaging thermomechanical fatigue loadings. Turbine blades are now frequently made of nickel-base superalloy single crystals, because of their excellent mechanical properties at high temperature, especially under creep loadings. Life prediction of these structures is a key feature for aerojet engines and gas turbines manufacturers. Present models are able to compute crack initiation time from elasto-viscoplastic finite element (FE) calculations. But these lifetime criteria are often too conservative: analyses performed on real structures have revealed that cracks may propagate and then stop, preserving the structure's integrity. The understanding of crack propagation in single crystal (SC) nickel-base superalloys is also necessary to predict crack growth rate as well as crack path.

The behaviour of such alloys has been extensively studied during the last twenty years, for various temperature ranges and loadings (fatigue, creep and creep-fatigue) [1–5]. It has been shown that these SC are prone to strain localization [1,6].

The life prediction of these structures has also been studied. Most studies focused on crack initiation and were also applied to life prediction of volume elements, under isothermal and non-isothermal loading conditions [7]. Crack propagation at low (i.e. <650 °C) and high (i.e. >750 °C) temperature was investigated in [8–10]. Crack bifurcation has been observed in some temperature ranges (Fig. 1). These works have pointed out some crack growth mechanisms, but most proposed models [7,11,12] were not designed to simulate explicitly crack growth.

The difficulty to get structure-oriented models with these approaches leads us to focus on local approaches. Such kinds of approaches require the accurate calculation of stress and strain in the vicinity of the crack-tip [13]. For single crystals, classical solutions such as HRR fields for polycrystalline materials are not valid anymore, because of the strongly anisotropic nature of plastic deformation. Actually, these SC nickel-base superalloys have a face centred cubic (fcc) crystallographic structure. Their plastic

* Corresponding author. Tel.: +33 1 60 76 30 51; fax: +33 1 60 76 31 50.
E-mail address: samuel.forest@ensmp.fr (S. Forest).

0927-0256/$ - see front matter © 2005 Elsevier B.V. All rights reserved.
doi:10.1016/j.commatsci.2005.12.014

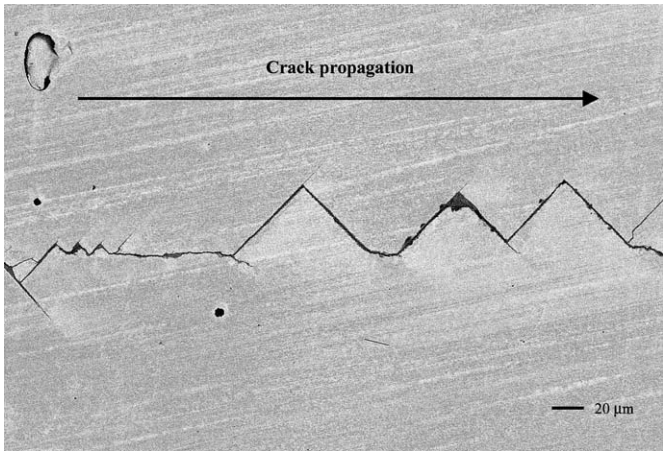

Fig. 1. Example of successive crack bifurcations in a (0 0 1)[1 1 0] CT specimen in fatigue ($T = 650$ °C).

deformation is due to plastic slip on 12 octahedral $\{1\,1\,1\}\langle 1\,1\,0\rangle$ and 6 cube $\{1\,0\,0\}\langle 1\,1\,0\rangle$ slip systems. In 1987, Rice [14] found the asymptotic solution for a (0 0 1)[1 1 0] crack orientation (where (0 0 1) is the crack plane and [1 1 0] the crack propagation direction), considering several assumptions: plane strain state, elastic–perfectly plastic material behaviour, mode I and monotonic loading. This results in four sectors (A, B, C, D), in which the Cartesian components of stress are constant (Fig. 2). Between each sector, there is a strain localization band. The number of these bands, as well as their orientation and nature, depend on the crystal orientation with respect to the crack orientation. For the (0 0 1)[1 1 0] crack orientation, the three bands AB, BC and CD are respectively at 54.7°, 90° and 125.3° from the crack propagation direction [1 1 0]. These bands will be used to indicate the location of plastic activation, but the results shown in this work strongly differ from the elastic–perfectly plastic case. The strain localization patterns at the crack-tip in SC have been extensively studied, numerically and experimentally [15–19]. A comprehensive analysis of crack orientations and localization patterns (including experimental observations) can be found in [17]. Such an analysis is important because strain localization seems to be related to crack bifurcation [16]. The influence of fatigue loading has been studied in [18], for elastic–perfectly plastic material behaviour. However, to the authors' knowledge, no work has been done for creep-fatigue loadings, considering high temperature material behaviour.

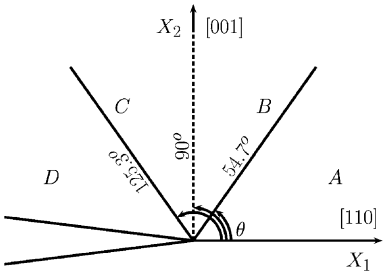

Fig. 2. Constant stress sectors.

In the first section of this paper, the elasto-viscoplastic constitutive model used for finite element simulations is presented. The mesh, boundary conditions and loading conditions are also presented. The second section shows the results obtained for creep-fatigue loading conditions and focuses on the differences with pure fatigue or pure creep loading conditions. The activation of slip systems is analysed around the crack-tip, and the evolution of slip as a function of time is shown for an octahedral slip system in front of the crack-tip.

2. Computational tools

2.1. Constitutive laws

Several models exist to describe the anisotropic behaviour of SC nickel-base superalloys, for a wide range of temperatures. It is possible to distinguish three main types of models:

- Phenomenological models, based on theory of invariants [2,20].
- Crystallographic phenomenological models [21,22].
- Crystallographic micromechanical models [23,24].

Here, the modelling of material behaviour is done using Cailletaud's crystallographic model [21], because of its low computational cost and its consistency with experimental results obtained for various crystal orientations. This model was calibrated for AM1 and CMSX4 single crystals under cyclic loadings by Hanriot [1] and Köster [7]. The classical partition of strain is assumed

$$\dot{\tilde{\varepsilon}} = \dot{\tilde{\varepsilon}}^{\mathrm{e}} + \dot{\tilde{\varepsilon}}^{\mathrm{p}} \tag{1}$$

Elastic strain is defined as

$$\tilde{\varepsilon}^{\mathrm{e}} = \tilde{\tilde{C}}^{-1} : \tilde{\sigma} \tag{2}$$

where $\tilde{\tilde{C}}$ is the fourth-order tensor of elastic moduli.

The flow rule is written at the slip system level and the macroscopic strain rate $\dot{\tilde{\varepsilon}}^{\mathrm{p}}$ is obtained with the orientation tensor $\tilde{m}^s$ (corresponding to Schmid law)

$$\tilde{m}^s = \frac{1}{2}\left(\vec{n}^s \otimes \vec{l}^s + \vec{l}^s \otimes \vec{n}^s\right) \tag{3}$$

where $\vec{n}^s$ is the normal to the plane of slip system s, and $\vec{l}^s$ is the slip direction of system s.

$$\dot{\tilde{\varepsilon}}^{\mathrm{p}} = \dot{\tilde{\varepsilon}}^{\mathrm{p}}_{\mathrm{oc}} + \dot{\tilde{\varepsilon}}^{\mathrm{p}}_{\mathrm{cu}} = \sum_{s=1}^{12} \tilde{m}^s \dot{\gamma}^s_{\mathrm{oc}} + \sum_{s=1}^{6} \tilde{m}_s \dot{\gamma}^s_{\mathrm{cu}} \tag{4}$$

The flow rule on slip system s is a classical Norton rule with threshold

$$\dot{\gamma}^s = \left\langle \frac{|\tau^s - x^s| - r^s}{k_I} \right\rangle^{n_I} \mathrm{sgn}(\tau^s - x^s) \tag{5}$$

where $I = 1$, 2 respectively for octahedral and cube slip systems.

Isotropic hardening is considered constant, and no interaction between slip systems is accounted for

$$r^s = r_{0_I} \tag{6}$$

Kinematic hardening is non-linear

$$x^s = c_I \alpha^s \tag{7}$$

with

$$\dot{\alpha}^s = \dot{\gamma}^s - d_I \dot{v}^s \alpha^s \quad \text{and} \quad \dot{v}^s = |\dot{\gamma}^s| \tag{8}$$

The viscoplastic behaviour is also described by five parameters for each family of slip systems: k_I, n_I, r_{0_I}, c_I, d_I with $I = 1$, 2. These coefficients were identified to simulate high temperature behaviour (950 °C) with important viscous effects and significant hardening.

Cumulative octahedral and cube slip variables are defined as

$$\dot{\gamma}^{\text{oc}}_{\text{cum}} = \sum_{s=1}^{12} |\dot{\gamma}^s_{\text{oc}}| \tag{9}$$

$$\dot{\gamma}^{\text{cu}}_{\text{cum}} = \sum_{s=1}^{6} |\dot{\gamma}^s_{\text{cu}}| \tag{10}$$

Shear stresses are defined as

$$\tau^s_{\text{oc}} = \tilde{m}^s_{\text{oc}} : \tilde{\sigma} \tag{11}$$

$$\tau^s_{\text{cu}} = \tilde{m}^s_{\text{cu}} : \tilde{\sigma} \tag{12}$$

2.2. Loading sequence, mesh and boundary conditions

The loading sequence is 1s monotonic loading/90s hold time/1s unloading (Fig. 3). The load ratio is defined as: $R = \frac{K_{\min}}{K_{\max}} = 0.1$ and $K_{\max} = 20\,\text{MPa}\sqrt{m}$, which are typical values for fatigue crack growth in superalloy SC. The orientation of the crack is (0 0 1)[1 1 0].

The 2D mesh (Fig. 4) is representative of a compact tension (CT) specimen, despite the fact that 3D meshes are in principle necessary to calculate plastic deformation in a CT specimen made of single crystal, as shown in [17]. This aims at saving computation time since many cycles will be simulated. The calculation is done under plane strain conditions. The mesh is a free mesh, except at the crack-tip, where 5 μm square quadratic elements are used. Possible crack–closure effects are accounted for using a "positive displacement" boundary condition along the crack. The calculations are done with an updated mesh geometry, with the assumption of small strains (they are not larger than 10%). All finite element simulations were performed with the FE code Z-Set, developed at Ecole des Mines de Paris, ONERA and Northwest Numerics (www.nwnumerics.com).

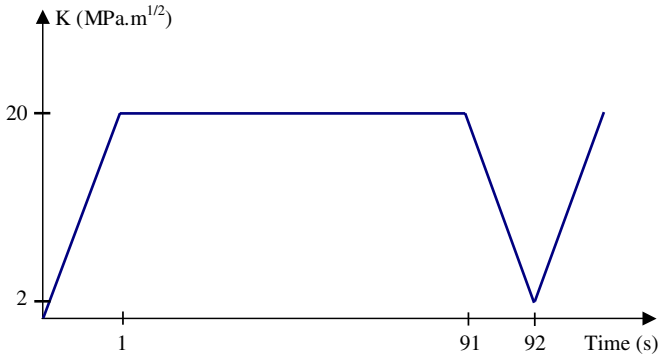

Fig. 3. Loading sequence.

3. Creep-fatigue loading conditions

3.1. Results

In Fig. 5, the cumulative octahedral slip $\gamma^{\text{oc}}_{\text{cum}}$ is plotted at three instants at the beginning of cycling. One can see that sectors B and D are activated. The largest increase of slip is obtained during the first dwell time. In Fig. 6, cumulated slip on octahedral and cube slip systems is plotted along a path surrounding the crack-tip at 35 μm (see path in Fig. 4), at the end of the first dwell time and of the second dwell time. A peak is clearly visible at nearly 90° and means that cube slip is activated in a vertical sector. The amount of cumulated plastic slip on cube slip systems is very large, which is unusual in fcc single crystals. For octahedral slip, peaks are less pronounced. However, a local maximum is reached at approximately 70–80° and another at nearly 135°. We define a front band, located at 75° from [1 1 0], i.e. where octahedral slip is predominant (Fig. 6).

Under plane strain conditions, plastic deformation in sector B (Fig. 2) is due to the simultaneous and symmetrical activation of two octahedral slip systems: $(1\,1\,\bar{1})[1\,0\,1]$ and $(1\,1\,\bar{1})[0\,1\,1]$. The activation of these two slip systems is equivalent to the activation of a $(1\,1\,\bar{1})$ [1 1 2] system, called "effective slip system" in [16]. The [1 1 2] direction is parallel to the plane defined by [0 0 1] and [1 1 0] and justifies the choice of the 2D mesh. Because of this symmetry, only octahedral slip system $(1\,1\,\bar{1})[1\,0\,1]$ (numbered 12 in Z-Set and on the figures) will be referred to. Hence, we analyse the evolution of slip and shear stress on this system at four points 1, 2, 3, 4 lying on the line at 75° (respective distances to the crack-tip ≈25, 50, 60 and 70 μm) (Fig. 4). In fact, this area is thought to be the most important for crack propagation, because it is located in front of the crack tip: plastic slip is this band tends to make the crack propagate. Crack propagation along {1 1 1} planes has been also evidenced experimentally, in some temperature ranges [25] (Fig. 1). Moreover, in the low temperature case, Flouriot has shown in [18] that for the (0 0 1)[1 1 0] crack orientation under pure fatigue loadings slip stops in the rear and vertical bands, whereas it is still activated in the front band.

In Fig. 7, the $\tau_{\text{oc12}} - \gamma_{\text{oc12}}$ loops at points 1–4 illustrate the stress relaxation behaviour of the material on system 12. Actually, the mean stress relaxation can be clearly seen and a trend of strain saturation around 0.8% at point 1 is

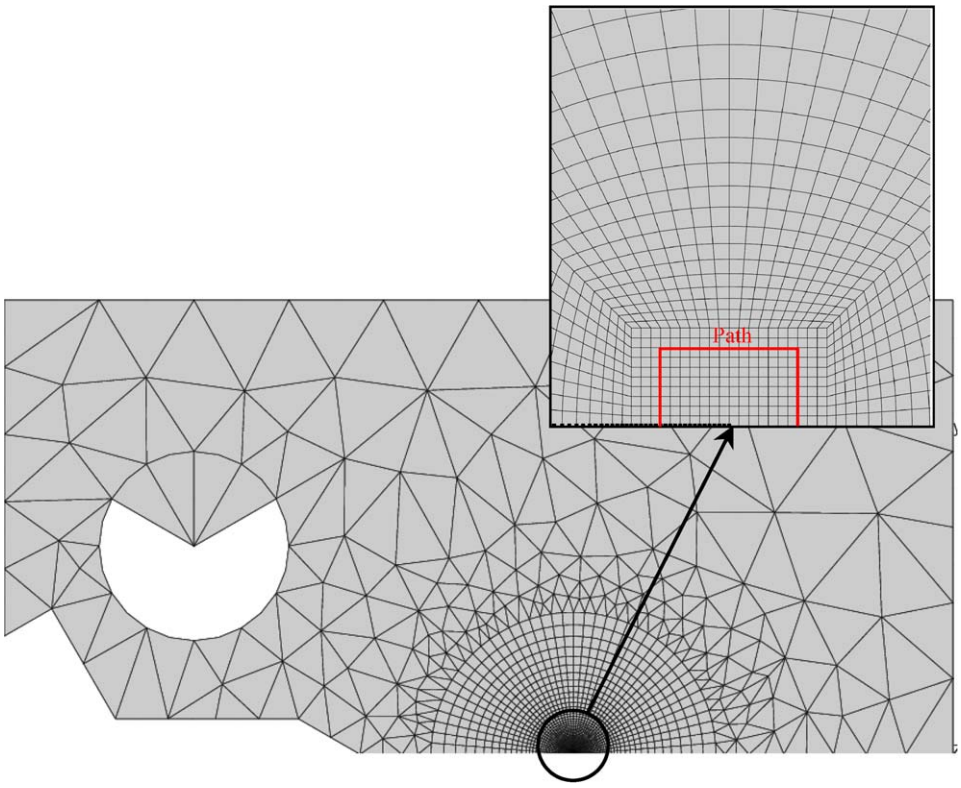

Fig. 4. View of the CT mesh used for FE analyses.

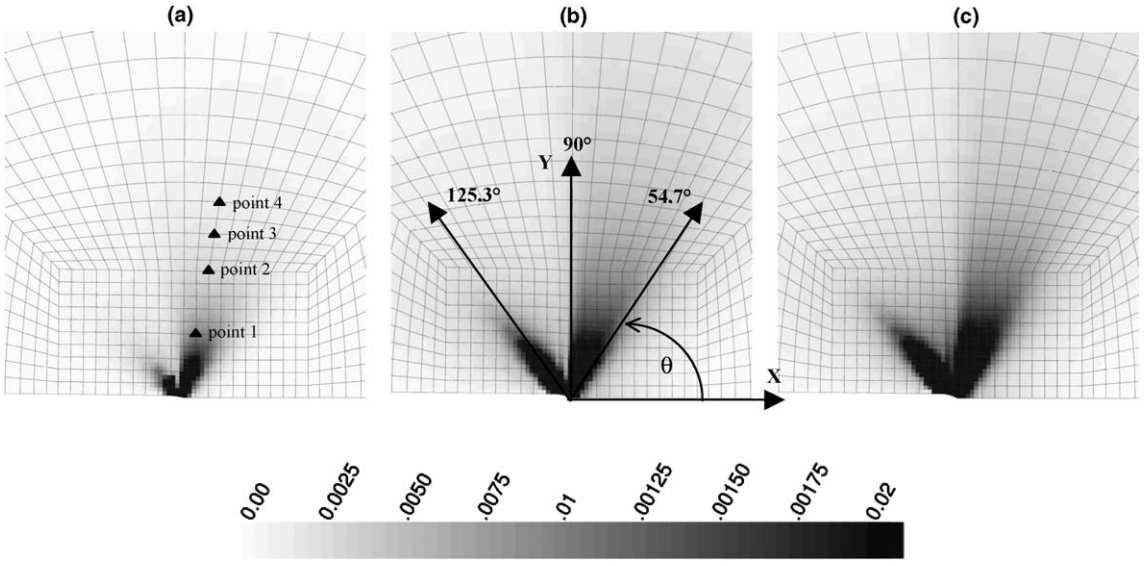

Fig. 5. Octahedral slip isovalues, at three times of the loading sequence: (a) beginning of the first dwell time, (b) end of the first dwell time and (c) end of the second dwell time.

observed. A ''local ratchetting effect'' can be observed, especially for points 2–4: this effect consists in the uninterrupted accumulation of plastic slip during cycling, despite reverse loadings (for point 1, this phenomenon occurs during the eight first cycles). Important stress relaxation during the first dwell time is observed.

In Fig. 8, plastic slip on system 12 is plotted as a function of time, for the points 1–4. The curves are rather different for point 1, point 2 and points 3–4, located further from the crack-tip. For point 1, the evolution of maximal plastic slip versus time is not monotonic. Actually, slip begins to increase at each cycle during the first eight cycles,

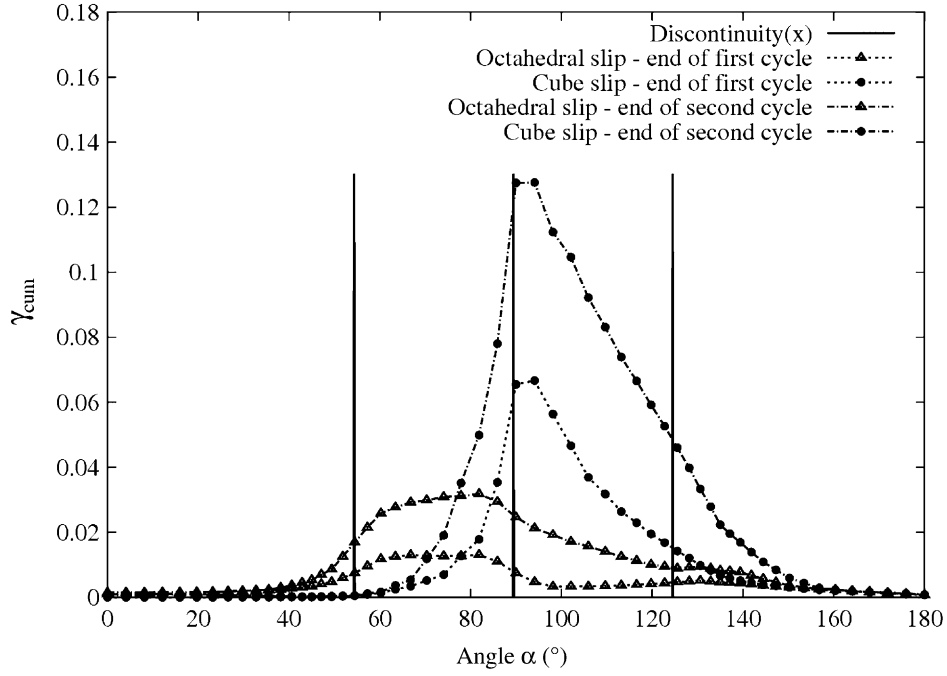

Fig. 6. Amount of slip along a path surrounding the crack-tip.

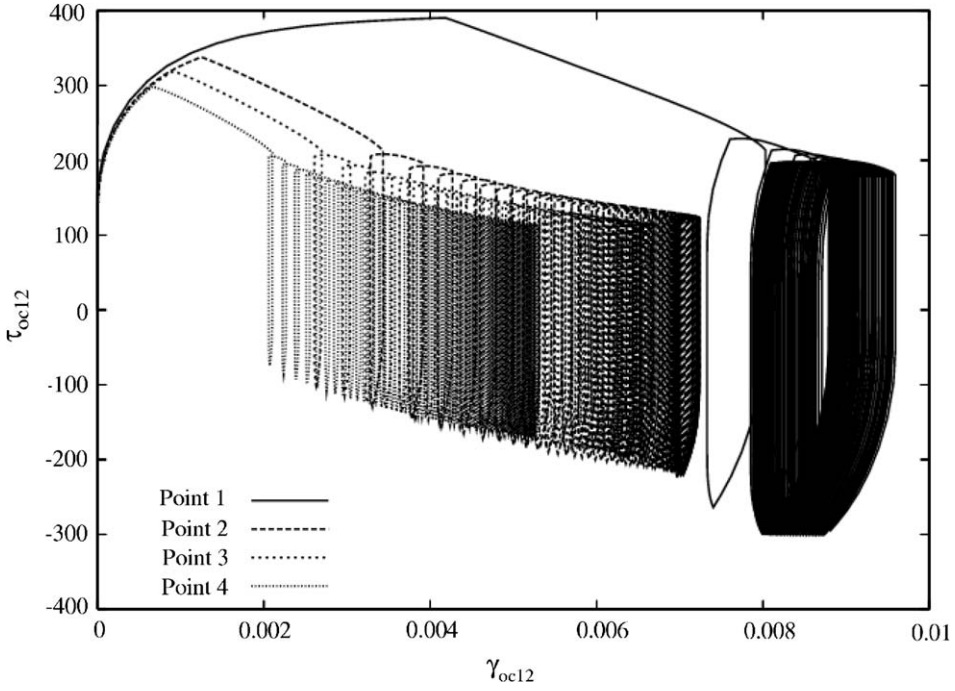

Fig. 7. Resolved shear stress as a function of slip on system 12, after more than 80 cycles.

up to a maximum. Then, it decreases up to $t = 4000$ s (≈ 43 cycles), and after that it rises again, reaching the maximum value again. Computations with higher cycle number are necessary to know whether this oscillatory behaviour goes on or stops at a stabilized cycle. For point 2, the local ratchetting effect can be observed again: slip increases at each cycle, and reaches a stabilized value after approximately 5000 s. For points 3 and 4, plastic slip still increases at every cycle, even after 80 loading cycles. The differences of slip evolution between these points can be explained by the fact that viscous stresses do not affect the material at points 3 and 4 yet, because they are located further from the crack-tip.

It is interesting now to check if similar results under creep-fatigue loadings can be observed for pure fatigue or pure creep loadings.

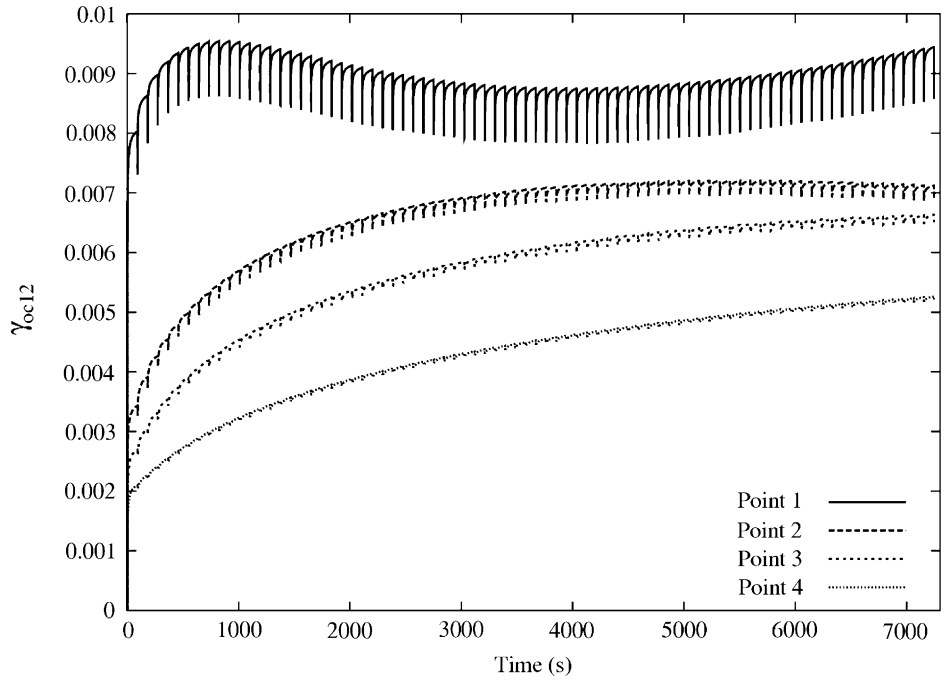

Fig. 8. Amount of slip on system 12 as a function of time at four points on the front band.

3.2. Comparison with pure fatigue and pure creep loadings

Pure fatigue loading ($R = 0.1$, $f = 0.5$ Hz, $K_{max} = 20\ \mathrm{MPa}\sqrt{m}$) and creep loading ($K = 20\ \mathrm{MPa}\sqrt{m}$) were applied to the same mesh to compare slip systems activity. Hundred fatigue cycles were calculated and creep is computed during 7500 s (i.e. longer than 80 creep-fatigue cycles).

The results of pure fatigue simulations are presented in Figs. 9 and 10. Fig. 9 shows the important differences between both loading conditions. Actually, not only the amounts of slip differ, but also the amount of stress relaxation. At point 1, stress reaches a stabilized value (Fig. 9)

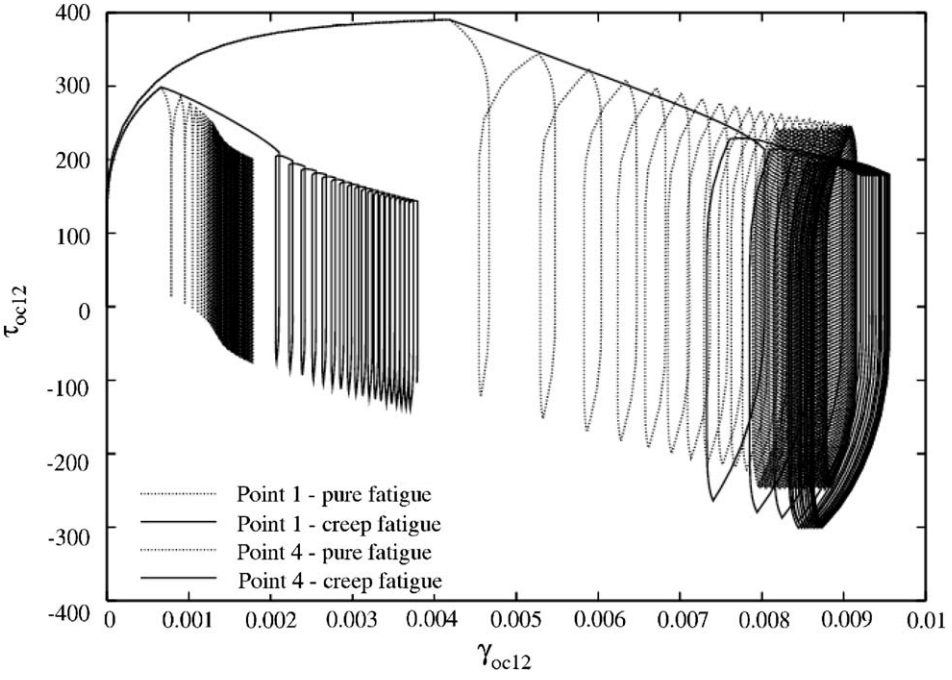

Fig. 9. Comparison between pure fatigue and creep-fatigue loadings. Resolved shear stress as a function of slip on system 12, at points 1 and 4, after 1840 s.

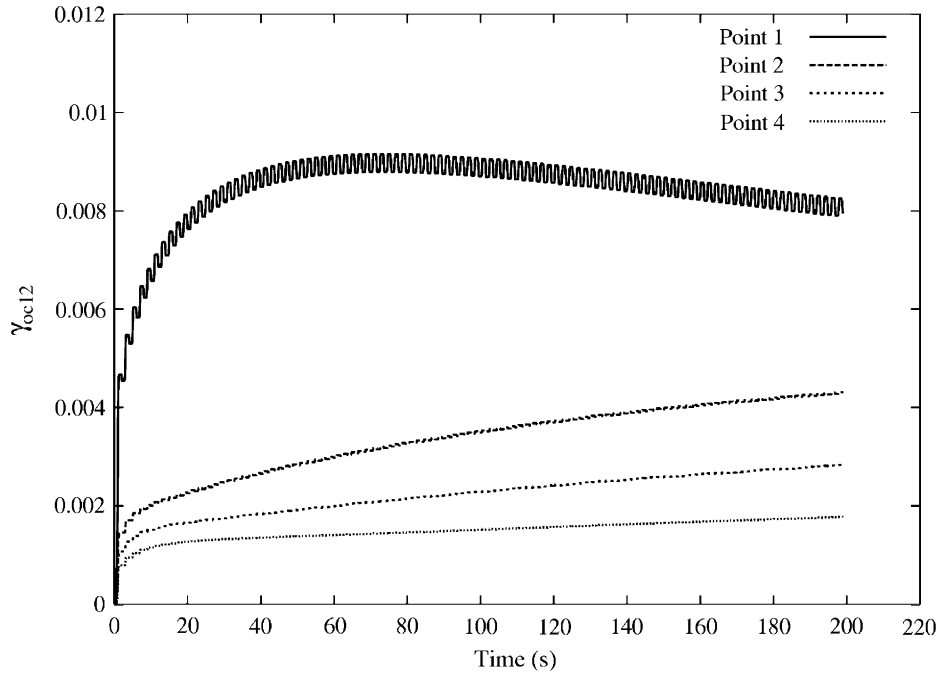

Fig. 10. Slip on system 12 as a function of time, for pure fatigue loading (100 cycles).

for both loadings. The value is much lower in the case of creep-fatigue because of the presence of dwell times, especially thanks to the first dwell time, which causes a large stress relaxation. In Fig. 10, we can see that the variation of slip as a function of time during each cycle is very different for pure fatigue and creep-fatigue: there is less slip during each fatigue cycle than during each creep-fatigue cycle. Like for creep-fatigue, the curve related to point 1 is different from the other curves. At point 1, slip increases during the first cycles (local ratchetting effect), reaches a maximum, and then decreases. This is not the case for slip at points 2–4 for pure fatigue loading. The maximum of slip is slightly lower for pure fatigue than for creep-fatigue ($\gamma_{oc12} = 0.0092$ for pure fatigue and $\gamma_{oc12} = 0.0094$ for creep-fatigue), but it is not reached at the same time, or after the same number of cycles.

The results of simulations for pure creep loading are presented in Fig. 11. The resolved shear stress on system

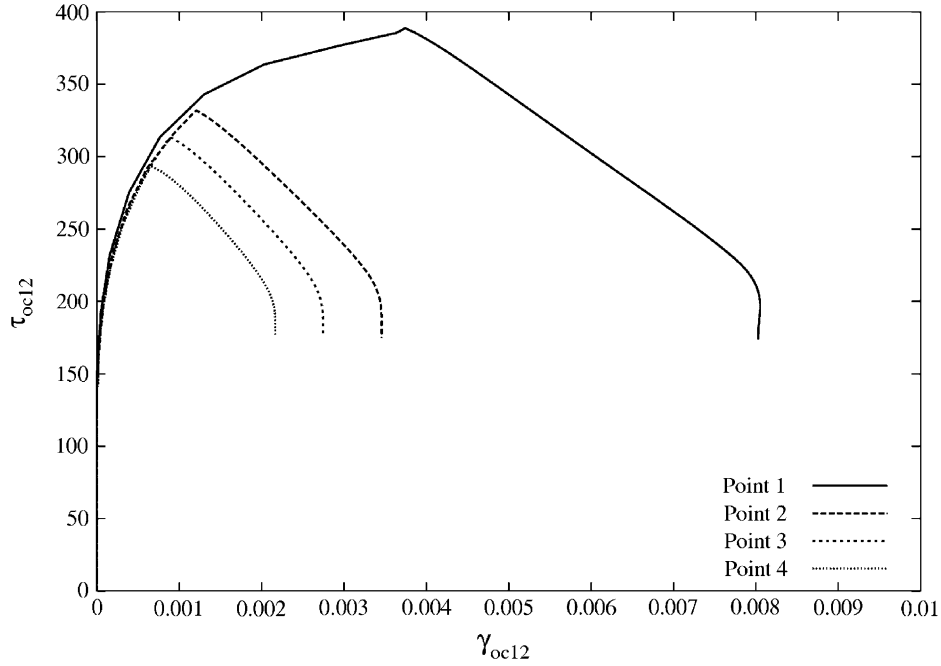

Fig. 11. Resolved shear stress as a function of slip on system 12 for pure creep loading.

12 decreases for each point, and reaches the same value for all points (end of each curve in Fig. 11). Slip at points 1–4 stabilizes very fast, at values that depend on the distance from the crack-tip (e.g. $\gamma_{oc12} \approx 0.008$ for point 1 and $\gamma_{oc12} \approx 0.002$ for point 4). The analysis of slip as a function of time on system 12 shows that the amount of slip at points 1 and 4 is much larger in the case of creep-fatigue than in the case of pure creep. Even the minimum value of maximal slip reached at $t = 4000$ s for point 1 (Fig. 8) is larger than the saturated value of slip due to creep (0.009 vs. 0.008).

4. Conclusions

This work focused on crack-tip stress and strain fields in a single crystal nickel-base superalloy. First, these fields were studied for a static crack subjected to creep-fatigue loading. They were then compared with stress–strain fields obtained for pure fatigue and pure creep loading conditions. We have shown that the stress–strain state at the tip of a static crack is very complex when considering viscoplastic material behaviour and complex loading conditions. Actually, the crack-tip stress–strain fields depend on the distance to the crack-tip.

We have shown that for viscoplastic single crystal behaviour:

- Deformation takes place in specific sectors.
- Local ratchetting effects appear on octahedral slip systems in front of the crack-tip.
- These ratchetting effects tend to stabilize, depending on the distance from the crack-tip.
- Creep-fatigue enables more stress relaxation than pure fatigue or pure creep on octahedral system $(11\bar{1})$ [101] in front of the crack-tip.

However, the validation of these results has to be done experimentally. For example, the experimental observation of the activation of viscoplastic sectors shall be done at high temperature. The main difficulty is the surface oxidation of the specimen, which necessitates carrying out the test under vacuum. Moreover, the fact that the crack remains static in our calculations has also to be checked for a real crack.

Acknowledgements

The support of the European Commission in the framework of SOCRAX research project (G5RD-CT-2002-00819) is gratefully acknowledged by the authors.

References

[1] F. Hanriot, G. Cailletaud, et al., Mechanical behaviour of a nickel-based superalloy single crystal, in: A.D. Freed, K.P. Walker (Eds.), High Temperature Constitutive Modelling—Theory and application, ASME, New York, 1991, pp. 139–150.

[2] D. Nouailhas, J.-P. Culié, Development and application of a model for single crystal superalloys, in: International Conference on High Temperature Constitutive Modeling, ASME, Atlanta, USA, 1991.

[3] D. Nouailhas, D. Pacou, et al., Experimental study of the anisotropic behaviour of the CMSX2 single crystal superalloy under tension–torsion loadings, in: D. McDowell, R. Ellis (Eds.), Advances in Multiaxial Fatigue, 1993, pp. 244–258.

[4] A. Cuitiño, M. Ortiz, Computational modeling of single crystals, Modelling and Simulation in Materials Science and Engineering 1 (1992) 225–263.

[5] S. Forest, P. Pilvin, Modelling the cyclic behaviour of two-phase single crystal nickel-base superalloys, in: A. Pineau, A. Zaoui (Eds.), IUTAM Symposium on Micromechanics of Plasticity and Damage of Multiphase Materials, Kluwer Academic, Netherlands, 1996, pp. 51–58.

[6] R. Chieragatti, Influence of orientation on the low cycle fatigue behaviour of MAR-M200 single crystals. Part II: cyclic stress–strain behaviour, Materials Science and Engineering, A 141 (1991) 11–22.

[7] A. Köster, A.M. Alam, et al., A physical-base model for life prediction of single crystal turbine blades under creep-fatigue loading and thermal transient conditions, in: Temperature–Fatigue Interaction, in: L. Rémy, J. Petit (Eds.), ESIS Publication 29, Elsevier, Paris, 2002, pp. 203–212.

[8] E. Fleury, L. Rémy, Low cycle fatigue damage in nickel-base superalloy single crystals at elevated temperature, Materials Science and Engineering A 167 (1993) 23–30.

[9] A. Defresne, L. Rémy, Fatigue behaviour of CMSX 2 superalloy [001] single crystals at high temperature II: fatigue crack growth, Materials Science and Engineering A 129 (1990) 55–64.

[10] M.B. Henderson, J.W. Martin, The influence of crystal orientation on the high temperature fatigue crack growth of a Ni-based single crystal superalloy, Acta Materialia 44 (1996) 111–126.

[11] F. Gallerneau, J.-L. Chaboche, Fatigue life prediction of single crystals for turbine blade applications, International Journal of Damage Mechanics 8 (1999) 405–427.

[12] J.-L. Chaboche, F. Gallerneau, An overview of the damage approach of durability modelling at elevated temperature, International Journal on Fatigue and Fracture of Engineering Materials and Structures 24 (2001) 405–418.

[13] J. Besson, C. Berdin, et al., Local Approach to Fracture, Ecole des Mines de Paris, Paris, 2004, p. 428.

[14] J.R. Rice, Tensile crack tip fields in elastic–ideally plastic crystals, Mechanics of Materials 6 (1987) 317–335.

[15] A. Cuitiño, M. Ortiz, Three-dimensional crack-tip fields in four-point-bending copper single-crystal specimens, Journal of the Mechanics and Physics of Solids 44 (1996) 863–904.

[16] S. Forest, P. Boudibi, et al., Strain localization patterns at a crack tip in generalized single crystal plasticity, Scripta Materialia 44 (2001) 953–958.

[17] S. Flouriot, S. Forest, et al., Strain localization at the crack tip in single crystal CT specimens under monotonous loading: 3D finite element analyses and application to nickel-base superalloys, International Journal of Fracture 124 (2003) 43–77.

[18] S. Flouriot, S. Forest, et al., Strain localization phenomena under cyclic loading: application to fatigue of single crystals, Computational Materials Science 26 (2003) 61–70.

[19] J.R. Rice, D. Hawk, et al., Crack tip fields in ductile single crystals, International Journal of Fracture 42 (1990) 301–321.

[20] S.X. Li, D.J. Smith, Development of an anisotropic constitutive model for single-crystal superalloy for combined fatigue and creep loading, International Journal of Mechanical Sciences 40 (1998) 937–948.

[21] L. Méric, P. Poubanne, et al., Single crystal modelling for structural calculations: Part 1—model presentation, Journal of Engineering Materials and Technology 113 (1991) 162–170.

[22] G. Cailletaud, Une approche micromécanique phénoménologique du comportement inélastique des métaux. Thèse d'état. Centre des Matériaux, Ecole Nationale Supérieure des Mines de Paris, 1987.

[23] B. Fedelich, A microstructural model for the monotonic and the cyclic mechanical behavior of single crystals of superalloys at high temperatures, International Journal of Plasticity 18 (2002) 1–49.
[24] E.P. Busso, F.T. Meissonnier, et al., Gradient-dependent deformation of two-phase single crystals, Journal of the Mechanics and Physics of Solids 48 (2000) 2333–2361.
[25] E. Fleury, Endommagement du superalliage monocristallin AM1 en fatigue isotherme et anisotherme. Ph.D. thesis. Centre des Matériaux, Ecole Nationale Supérieure des Mines de Paris, 143pp, 1991.